Accepted Manuscript

Dextran sulfate nanoparticles as a theranostic nanomedicine for rheumatoid arthritis

Roun Heo, Dong Gil You, Wooram Um, Ki Young Choi, Sangmin Jeon, Jong-Sung Park, Yuri Choi, Seunglee Kwon, Kwangmeyung Kim, Ick Chan Kwon, Dong-Gyu Jo, Young Mo Kang, Jae Hyung Park

PII: S0142-9612(17)30201-6

DOI: 10.1016/j.biomaterials.2017.03.044

Reference: JBMT 18014

To appear in: *Biomaterials*

Received Date: 19 January 2017

Revised Date: 24 March 2017

Accepted Date: 25 March 2017

Please cite this article as: Heo R, You DG, Um W, Choi KY, Jeon S, Park J-S, Choi Y, Kwon S, Kim K, Kwon IC, Jo D-G, Kang YM, Park JH, Dextran sulfate nanoparticles as a theranostic nanomedicine for rheumatoid arthritis, *Biomaterials* (2017), doi: 10.1016/j.biomaterials.2017.03.044.

<*Manuscript for Biomaterials*>

Dextran Sulfate Nanoparticles as a Theranostic Nanomedicine for Rheumatoid Arthritis

Roun Heo[a,1], Dong Gil You[b,c,1], Wooram Um[a,c], Ki Young Choi[b], Sangmin Jeon[b], Jong-Sung Park[d], Yuri Choi[e], Seunglee Kwon[b], Kwangmeyung Kim[c], Ick Chan Kwon[c], Dong-Gyu Jo[e], Young Mo Kang[f], and Jae Hyung Park[a,b,*]

[a] Department of Health Sciences and Technology, SAIHST, Sungkyunkwan University, Seoul 06351, Republic of Korea

[b] School of Chemical Engineering, College of Engineering, Sungkyunkwan University, Suwon 16419, Republic of Korea

[c] Center for Theragnosis, Biomedical Research Institute, Korea Institute of Science and Technology, Seoul 02792, Republic of Korea

[d] Department of Radiology and Radiological Science, Johns Hopkins University, Baltimore 21231, United States

[e] School of Pharmacy, Sungkyunkwan University, Suwon 16419, Republic of Korea

[f] School of Medicine, Kyungpook National University, Daegu 41566, Republic of Korea

[1] These authors contributed equally to this work.

*Corresponding author:

Jae Hyung Park, Ph.D.

Tel: +82-31-290-7288; fax: +82-31-292-8790; e-mail: jhpark1@skku.edu

Abstract

With the aim of developing nanoparticles for targeted delivery of methotrexate (MTX) to inflamed joints in rheumatoid arthritis (RA), an amphiphilic polysaccharide was synthesized by conjugating 5β-cholanic acid to a dextran sulfate (DS) backbone. Due to its amphiphilic nature, the DS derivative self-assembled into spherical nanoparticles (220 nm in diameter) in aqueous conditions. The MTX was effectively loaded into the DS nanoparticles (loading efficiency: 73.0 %) by a simple dialysis method. Interestingly, the DS nanoparticles were selectively taken up by activated macrophages, which are responsible for inflammation and joint destruction, via scavenger receptor class A-mediated endocytosis. When systemically administrated into mice with experimental collagen-induced arthritis (CIA), the DS nanoparticles effectively accumulated in inflamed joints (12-fold more than wild type mice (WT)), implying their high targetability to RA tissues. Moreover, the MTX-loaded DS nanoparticles exhibited significantly improved therapeutic efficacy against CIA in mice compared to free MTX alone. Overall, the data presented here indicate that DS nanoparticles are potentially useful nanomedicines for RA imaging and therapy.

Keywords: Dextran sulfate, nanoparticles, drug delivery, macrophage, rheumatoid arthritis.

1. Introduction

Rheumatoid arthritis (RA) is a complex chronic inflammatory disease characterized by increased vascular permeability and the consequential invasion of immune cells such as activated macrophages and lymphocytes [1-3]. Although the precise cause of RA remains unknown, activated macrophages have been found to be the most prominent cells in the inflamed joints of patients with RA and are believed to make a major contribution to articular inflammation and joint damage pathogenesis [4, 5]. Therefore, the targeting of activated macrophages and inflammatory cytokines such as tumor necrosis factor-α has been considered an effective way to relieve symptoms of RA [5, 6].

Methotrexate (MTX), a disease-modifying anti-rheumatic drug, has been widely used both alone and in combination with biologics to treat RA. However, due to its extensive and random distribution in the body, MTX often causes serious side effects such as hair loss, nausea, headaches, and skin pigmentation [7]. In fact, half of all MTX-treated patients experience side effects, which limit the long-term use and tolerability of this drug [8]. One strategy for overcoming this challenge is to develop nanocarriers for MTX that target the drug to activated macrophages in the inflamed regions of RA and reduces the fraction of drug reaching toxicological targets.

Nanomedicine has emerged as promising therapeutics for treatment of intractable diseases such as atherosclerosis and cancer because nanoparticles exhibit unique properties including (i) prolonged circulation in the bloodstream followed by systemic accumulation at the disease site, (ii) visualization of target tissues or molecular events in the tissues, (iii) targeted drug delivery to the target tissues, and (iii) controlled drug release at desired action sites, [9-12]. In recent years, polymeric nanoparticles have been employed for RA therapy because they can

passively accumulate into inflamed synovial tissues due to the leaky nature of the vasculature [13-15]. Moreover, the therapeutic efficacy of these nanoparticles can be significantly enhanced by using nanocarriers capable of recognizing their target cells via specific receptor-ligand interactions [16, 17].

In the early stage of RA, activated macrophages exhibit significant overexpression of scavenger receptors, which can bind and internalize oxidized low-density lipoprotein and polyanionic macromolecules [18-20]. Dextran sulfate (DS) and its derivatives have received increasing attention in biomedical applications because of their remarkable biocompatibility and biodegradability [21-23]. Notably, DS acts as a ligand for macrophage scavenger receptor class A (SR-A), which is overexpressed by activated macrophages [24, 25]. Therefore, we hypothesize that DS-based nanoparticles might effectively reach inflamed joints by both passive and active targeting mechanisms, making them ideal drug carriers for RA therapy.

To effectively deliver MTX to the inflamed joints in RA, we prepared DS nanoparticles (DSNPs) consisting of a DS hydrophilic shell and a hydrophobic drug reservoir of 5β-cholanic acid. We hypothesized that the DS surface of the nanoparticle allows for specific binding to SR-A on activated macrophages, followed by receptor-mediated endocytosis and intracellular release of MTX (Fig. 1). The physicochemical characteristics of DSNPs (e.g. particle size and morphology) and their *in vitro* cellular uptake were monitored using macrophages and endothelial cells. To assess RA targetability, we examined the *in vivo* biodistribution of DSNPs after their systemic administration into mice with collagen-induced arthritis (CIA). In addition, the therapeutic effects of MTX-loaded DSNPs were evaluated by measuring the extents of synovitis, bone destruction, and cartilage destruction in mice with CIA. The potential of DSNPs as imaging probes to determine therapeutic efficacy was also

investigated by observing the extent of fluorescence in the inflamed joints. This study demonstrates for the first time that DSNPs can potentially be used for imaging and therapy of RA.

2. Materials and Methods

2.1. Materials

DS sodium salt (MW = 36 – 50 kDa) was purchased from MP Biomedicals, LLC (Aurora, OH, USA). 4-Nitrophenyl chloroformate, 4-dimethylamino pyridine (DMAP), methotrexate, and 5β-cholanic acid were obtained from Sigma-Aldrich Co. (St. Louis, MO, USA). The near-infrared fluorescence (NIRF) dye FPR-675 was purchased from DKC Corporation (Incheon, Korea). All other chemicals were of analytical grade and used without further purification. Macrophages (RAW264.7) and bovine aortic endothelial cells (BAECs) were purchased from the American Type Culture Collection (Rockville, MD, USA). All experimental involving live animals were carried out in accordance with the relevant laws and institutional guidelines of Sungkyunkwan University. The Sungkyunkwan University institutional committees have approved all the experimental protocols.

2.2. Synthesis of the amphiphilic DS derivative

The amphiphilic DS derivative was synthesized by conjugation of the hydrophobic 5β-cholanic acid to the hydrophilic DS backbone. Briefly, DS (100 mg, 0.262 mmol) and 4-nitrophenyl chloroformate (158 g, 0.786 mmol) were dissolved in dimethyl sulfoxide (DMSO)/pyridine (15 mL, 1/1(v/v)), and DMAP (9.6 mg, 0.0786 mmol) was added as a

catalyst [26]. The reaction mixture was stirred under argon for 4 h at 0°C. The reaction product was then precipitated in 300 ml of diethyl ether/ethanol (1/1, v/v), filtered, and washed with an excess amount of diethyl ether. Aminoethyl 5β-cholanic acid (13.81 mg, 0.0356 mmol), prepared as reported previously [17], was added to 10 mL of DMSO/pyridine (2/1, v/v) containing 4-nitrophenyl-activated dextran sulfate (100 mg, 0.178 mmol). The reaction mixture was stirred under argon for 48 h at 50°C. After the solution was concentrated, the product was dialyzed against excess water using a dialysis membrane (Spectra/Por®6, MWCO = 12 – 14 kDa) for 72 h. The chemical structure of the amphiphilic DS was characterized using an ^{1}H-NMR instrument (DD2 600 MHz FT NMR, Agilent Technologies, Santa Clara, CA, USA), for which the polymer was dissolved in $CD_3OD/D_2O/(CD_3)_2SO$.

2.3 Preparation and characterization of drug-loaded nanoparticles

MTX-loaded DSNPs (MTX-DSNPs) were prepared by a simple dialysis method as follows: First, amphiphilic DS (100 mg) was dissolved in 20 ml of anhydrous THF/distilled water (1/1, v/v). After addition of MTX (11.1 mg), the mixture was sonicated for 3 min at 4°C using a probe type sonicator (VCX-750, Sonics & Materials, Newtown, CT, USA) and dialyzed (Spectra/Por®6, MWCO = 6-8 kDa) against distilled water for 12 h to remove unloaded MTX molecules. The purified solution was filtered (0.8 μm syringe filter) and lyophilized to obtain a yellow powder. To quantify the amount of MTX encapsulated in DSNPs, we broke down the nanostructure of MTX-DSNPs to the soluble MTX and DS conjugate by dissolving MTX-DSNPs in the co-solvent of THF and distilled water (1/1, v/v). The amount of the MTX in the solution was determined by measuring the absorbance of MTX at 303 nm using a UV-vis spectrophotometer (Optizen 3220UV, Mecasys Co., Ltd., Daejeon, Korea) and calculated

based on the calibration curve. For the calculation of loading efficiency, we used the following calculation:

Encapsulation efficiency (%) = (weight of loaded MTX/weight of MTX in feed) x 100

For *in vitro* and *in vivo* fluorescence imaging, DSNPs were labeled with FPR-675 (λem = 675nm, λex = 720nm). In brief, DSNPs and FPR-675 were stirred in phosphate buffer (10 mM, pH 8.0) for 24 h at room temperature. The resulting solution was dialyzed (Spectra/Por® 6 MWCO = 6-8 kDa) against distilled water for 3 days, followed by lyophilization. As a control, dextran-based nanoparticles (Dex-NP) were prepared in an identical manner.

The hydrodynamic sizes and zeta potentials of the nanoparticles were measured at 1mg/ml concentration in distilled water (pH 6.5) using a Zeta-sizer instrument (Nano ZS, Malvern, UK), for which the nanoparticles were diluted in distilled water. The morphologies of the nanoparticles were obtained by transition electron microscopy (TEM, CM30, Philips, CA, USA). For TEM measurement, nanoparticles were dropped on a 400-mesh copper grid and stained with 5 % (W/V) uranyl acetate solution. The surface properties of DSNPs were characterized by using energy dispersive X-ray spectroscopy (EDS).

2.4 *In vitro* drug release behavior and cellular uptake of the nanoparticles

To assess their drug release behavior *in vitro*, MTX-DSNPs were dispersed in PBS (pH 7.4) and transferred to a cellulose membrane tube (Spectra/Por®6, MWCO = 6-8 kDa). The dialysis tube was then placed in the release medium and shaken at 100 rpm in a water bath at 37^{o}C. At predetermined time intervals, the release medium was refreshed by transferring the tube into the fresh release medium. The extent of cumulative drug release was then

determined by measuring the absorbance at 303 nm using a UV-vis spectrophotometer.

The cellular uptake of the DSNPs was evaluated using macrophages (RAW264.7) and endothelial cells (BAECs). RAW264.7 macrophages were cultured in high glucose DMEM (Welgene Inc., Daegu, Korea) containing 10 % FBS and 1% antibiotic–antimycotic solution (10,000 units/ml penicillin, 10 mg/ml streptomycine and 25 ug amphotericin B, Welgene Inc., Daegu, Korea) at 37^{o}C in a humidified 5 % CO_2 atmosphere. BAECs were cultured in low glucose DMEM with 20 % FBS and 1 % antibiotic–antimycotic solution at 37^{o}C in a 5 % CO_2 atmosphere. Cells were seeded into 35-mm cover slide bottom dishes (2 x 10^5 cells/dish) and maintained for 48 h. RAW264.7 macrophages were activated with lipopolysaccharide (LPS, 100 ng/ml) for 48 h. The medium was then replaced with 2 ml of serum-free medium containing FPR-675-DSNPs (100 µg/ml), followed by an incubation at 4^{o}C or 37^{o}C for 15 min or 30 min. The cells were then washed with PBS (pH 7.4) and fixed with 4% paraformaldehyde.

To confirm the SR-A-mediated endocytosis of DSNPs, the LPS treated RAW 264.7 cells were exposed 2 ml of serum-free medium containing the free DS polymer (5 mg/ml) for 60 min. Then, the cells were incubated with FPR-675-DSNPs and FPR-675-Dex-NPs for additional 30 min. The intracellular localization of the nanoparticles was observed using a confocal laser microscope (Leica TCS SP8, Leica Microsystems GmbH, Germany) with 405 diode (405 nm), Ar (458, 488, 514 nm), and He-Ne (633nm) lasers.

2.5. *In vivo* biodistribution of the nanoparticles

The CIA animal model consisted of male DBA1/J mice (6-8 weeks old) prepared as previously described [27, 28]. Briefly, mice were injected intradermally at the tail with 200

μg of bovine type II collagen (CII) (2 mg/ml, Chondrex, Redmond, WA, USA) emulsified in 100 μl of Complete Freund's Adjuvant (4 mg/ml). On day 21, mice received a booster immunization of CII emulsified in Incomplete Freund's Adjuvant. At 42 days after the primary immunization, FPR-675-DSNPs were injected into the tail vein of wild-type (WT) or CIA mice at a dose of 5 mg/kg. The time-dependent *in vivo* biodistribution was then observed using a Spectral Ami X imager (Spectral Instruments Imaging, Tucson, AZ, USA). Fluorescence images were obtained using wavelengths of 675 nm (excitation) and 730 (emission). NIRF images were quantified using Image-Pro Plus (Media Cybernetics, Rockville, MD, USA). Organs were dissected at 48 h after systemic administration of nanoparticles. *Ex vivo* fluorescence images were obtained using the Optix MS3 system (ART Advanced Research Technologies Inc., Montreal, Canada). The laser power and count time settings were optimized to 3 μW and 0.3 s per point.

For immunohistochemical analysis of inflamed joints in the CIA model, dissected knee joints were fixed in 10 % neutral buffered formalin before decalcification for 6 h using Decalcified Solution-Lite (Sigma-Aldrich Co.). Paraffin sections of the knee joints were then cut into 5 μm slices. The tissue sections were retrieved and immunostained with monoclonal anti-SR-A antibodies (Biorbyt Ltd, Cambridge, UK) and fluorescence-conjugated secondary antibodies (Alexa-488: Molecular Probes®, Eugene, OR, USA) according to the manufacturer's instructions. Fluorescence images were obtained using an LSM 510 MetaDuoScan confocal microscope (Carl Zeiss Micro Imaging GmbH, Jena, Germany).

2.6. *In vivo* and *ex vivo* fluorescence imaging

At 42 days after the primary immunization, 200 μl of FPR-675-DSNPs and FPR-675-Dex-

NPs were injected into the tail vein of CIA mice at a dose of 5 mg/kg. The time-dependent *in vivo* biodistribution was then observed using a IVIS Lumina III In Vivo imaging system (Caliper Life Science, Hopkinton, MA, USA). Fluorescence images were obtained using wavelengths of 660nm (excitation) and 710 (emission). NIRF images were quantified using embedded software.

2.7. Therapeutic efficacy of drug-loaded nanoparticles

The CIA mice were treated by intravenous injection of 200 μl of MTX (2.5 mg/kg), MTX-DSNPs (2.5 mg MTX/kg), empty DSNPs, or vehicle (PBS) once every four days, starting on the day of the booster injection. Each treatment was injected at 21, 25, 29, 33, and 37 days. Mice were monitored every other day to measure joint inflammation, scored as follows: 0 = normal, 1 = mild swelling and erythema confined to the midfoot and ankle joint, 2 = mild swelling and erythema extending to the midfoot and ankle joint, 3 = moderate swelling and erythema extending from the metatarsal joints to the ankle, 4 = severe swelling and erythema encompassing the foot, ankle, and digits. These paw scores were summed for each mouse, giving a maximum possible score of 16 [29]. Paw thickness for both the right and left paws was determined using calipers. For histological analysis, dissected knee joints were fixed in 10 % (v/v) buffered formalin solution, decalcified using Decalcified Solution-Lite for 6 h, embedded in paraffin, and sliced into 5 mm-thick sections. Sections were stained with H&E and examined under a fluorescence microscope (BX51, Olympus, Optical Co. Ltd., Tokyo, Japan). The extents of synovitis, bone destruction, and cartilage destruction were evaluated using a five-point scale as follows: grade 0 (no signs of inflammation), grade 1 (mild inflammation with minimal hyperplasia of the synovial lining layer without cartilage

destruction), and grades 2 through 4 (increasing degrees of inflammatory cell infiltration or cartilage and bone destruction).

2.8. Evaluation of the therapeutic effects of DSNPs

To evaluate the therapeutic effects of the DSNPs, the mice were divided into four groups: (a) WT, (b) non-treated CIA (non-boosted mice, 21 days), (c) non-treated CIA (boosted mice, 38 days), and (d) MTX-DSNP-treated CIA mice (boosted mice, 38 days). MTX-DSNPs (2.5 mg/kg of MTX) were injected intravenously into CIA mice. The MTX-DSNP treatment schedule was the same as above (5 injections at a time, once every three days). After receiving the MTX-DSNPs, all mice were injected intravenously with FPR-675-DSNPs (5 mg/kg). At 12 hours post-injection of the FPR-675-DSNPs, the skin of the knee joint was removed from each mouse and the extent of nanoparticle accumulation was monitored. Fluorescence images were obtained using an OV-100 small animal imaging system (Olympus, Center Valley, PA, USA) set to the bright field and the Cy5.5 channel (λex = 620–650 nm with λem = 680–710 nm). Immunohistochemical staining was performed by incubation with monoclonal anti-CD31 antibodies (1:200 dilution; Abcam, Cambridge, UK) at room temperature for 2 h. A Dako REAL EnVision Detection System (Dakocytomation, Carpinteria, CA, USA) was according to the manufacturer's instructions. The 5 μm-thick slides were counterstained with hematoxylin (Sigma), after which images were captured using an OLYMPUS BX51 microscope (Olympus, Tokyo, Japan).

2.9. Statistical analysis

The statistical significance among the groups was analyzed using one-way ANOVA.

Differences with a p value <0.05 were considered to be statistically significant. Statistical significance was assigned for $^{*}p$ <0.05, $^{**}p$ <0.01 and $^{***}p$ <0.001.

3. Results

3.1. Preparation and characterization of DSNPs

One strategy for increasing the therapeutic efficacy of MTX is to develop nano-sized carriers that can effectively accumulate at inflamed joints and release MTX inside the target cells. To prepare an amphiphilic DS derivative capable of forming self-assembled nanoparticles as a potential carrier of MTX, DS was chemically modified with aminoethyl 5β-cholanic acid by a simple two-step procedure (Fig. 2a). In this procedure, the hydroxyl group of DS was reacted with 4-nitrophenyl chloroformate, followed by conjugation of aminoethyl 5β-cholanic acid via amide bond formation. The chemical structure of the DS derivative was confirmed by inspection of the ^{1}H NMR spectrum, which showed the anomeric proton peak of DS at 5.27 ppm, the phenyl group peaks of 4-nitrophenyl chloroformate at 7.8 and 8.7 ppm, and the methyl group peak of aminoethyl 5β-cholanic acid at 0.9 ppm (Supplementary Fig. S1). The degree of substitution, defined as the number of aminoethyl 5β-cholanic acid per 100 sugar residues of DS, was estimated to be 9. It was calculated based on the integration ratio of the anomeric proton peak of DS at 5.27 ppm and methyl group peak of aminoethyl 5β-cholanic acid at 0.9 ppm.

The DSNPs had a unimodal size distribution (220.0 ± 5.17 nm) and a spherical shape (Fig. 2b and Supplementary Fig. S2). Elements of C(red), O(green) and S(blue), which represent the dextran sulfate polymer on the nanoparticles, were detected by the elemental mapping

analysis (Supplementary Fig. S3). In particular, strong signals of S (blue) on the nanoparticles verify that the dextran sulfate was located on the surface of the DSNP nanoparticles. Also we confirmed the long-term colloidal stability of DSNPs. DSNPs maintain the hydrodynamic size in PBS (pH 7.4) for at least 7 days (Supplementary Fig. S4). Moreover, DSNPs showed no significant size changes in the 10% FBS containing condition for 12 h. After 12 h post-incubation, DSNPs had a hydrodynamic size of 222.45 ± 21.62 nm. The zeta potential value of the DSNPs was highly negative (-47.5 ± 1.26 mV), which might be due to the DS sulfate groups on the nanoparticle surface. Hydrophobic MTX was readily encapsulated into the DSNPs by the dialysis method. The encapsulation efficiency and MTX content of the MTX-DSNPs prepared in this study were 73.0 % and 73ug/mg, respectively (Table 1). The DSNPs decreased in size to 173.4 ± 4.12 nm after MTX encapsulation, implying the formation of compact nanoparticles [30]. Next, the *in vitro* drug release kinetics of the nanoparticles were determined for two days in PBS (pH 7.4) (Fig. 2c). MTX was rapidly released from the DSNPs in the initial 3 h (51.8 ± 2.97%), followed by sustained release for the remaining period of time.

3.2. *In vitro* cellular uptake of the DSNPs

To evaluate the cellular uptake of the DSNPs, RAW264.7 macrophages and BAEC endothelial cells were treated with FPR-675-labeled DSNPs (red). In these experiments, macrophages were activated with LPS to induce the upregulation of the DS receptor SR-A [31]. Fluorescence images show that DSNPs were not significantly internalized into the RAW 264.7 (LPS +), RWA 264.7 (LPS -), and BAEC cells at 4^{o}C. However, after incubation of RAW264.7 cells (LPS +/-) and BAEC cells with DSNPs at 37^{o}C, strong fluorescence signals

were detected in RAW264.7 cells (LPS +). Significantly weaker fluorescence signals were observed in RAW264.7 cells (LPS -) than those in RAW264.7 (LPS +). Noticeable fluorescence intensities were not detected in BAEC cells incubated with DSNPs at 37^{o}C (Fig 3a and Supplementary Fig. S5). The results clearly demonstrate that cellular uptake mechanism of DSNPs is energy-dependent, SR-A-mediated endocytosis. Interestingly, no significant fluorescent signals were observed in the cells pretreated with the DS polymer, and treated with FPR-675-labeled DSNPs (DS pretreat) as well as in the cells treated with FPR-675-labeled Dex-NPs (Dex-NPs). On the other hand, strong DSNP fluorescent signals were observed when the cells treated with FPR-675-labeled DSNPs without pretreatment of DS polymer (Fig. 3b). These results suggest that DSNPs were effectively internalized into the activated macrophages through SR-A-mediated endocytosis.

3.3. *In vivo* biodistribution of the DSNPs

Next, the *in vivo* biodistribution and RA-targeting ability of the DSNPs were investigated using an optical imaging system after intravenous injection of FPR-675-labeled DSNPs into WT and CIA mice. Real-time NIRF images of the whole hind legs were obtained over time up to 48 h. No significant fluorescence was observed in the legs of the WT mice for 48 h (Fig. 4a). On the other hand, strong DSNP fluorescence was observed in the legs of CIA mice. Moreover, the inflamed joints were clearly discriminated from the surrounding normal tissues. In particular, the fluorescence intensity gradually increased at the inflamed joints over time, with a maximum intensity reached at 12 h post-injection, implying high RA targetability of the DSNPs.

Ex vivo NIRF images of the organs and joints of WT and CIA mice were obtained at 48 h

post-injection (Fig. 4b). For both WT and CIA mice, considerable fluorescence was detected in the liver and kidney, which might be due to uptake by the reticuloendothelial system and renal clearance of the nanoparticles, respectively. Interestingly, in CIA mice, the knee and ankle showed stronger fluorescence than all the other organs, indicating that most of the DSNPs accumulated in the inflamed joints. Quantitative analysis of the NIRF intensities revealed that the ankles and knees of CIA mice had approximately 12-fold and 6-fold more DSNPs than those of WT mice (Fig. 4c). These results suggest that DSNPs can effectively reach the inflamed joints of mice with RA, perhaps via the enhanced permeability and retention effect [32].

To further confirm the involvement of the SR-A in DSNP uptake, we examined the tissue distributions of the SR-A and DSNPs by immunohistochemistry (Fig. 5). Images of the knee joints of WT and CIA mice were obtained at 48 hours post-injection. As expected, the activated macrophage receptor SR-A was upregulated in the inflamed synovium of CIA mice compared with the synovium of WT mice. Interestingly, significant DSNP fluorescence was detected in the inflamed synovium; this fluorescent signal also colocalized with that of SR-A.

To clearly demonstrate active targeting effects on RA targetability of the nanoparticles, we further investigated the *in vivo* biodistribution and RA targeting activity of DSNPs in comparison with those of Dex-NPs in CIA mice (Fig. 6a). Interestingly, the inflamed tissues of the mice injected with DSNPs showed stronger fluorescence signals than those treated with Dex-NPs. At 12 h post-injection, DSNPs accumulated in the inflamed tissues of CIA mice 2-fold more than Dex-NPs (Fig. 6b). In particular, the fluorescence intensity of Dex-NPs gradually decreased at the inflamed joints over time, whereas the fluorescence intensity of DSNPs increased and remained strong up to 12 h. These results indicate that both DSNPs

and Dex-NPs can accumulate at inflamed joints by the passive targeting, but DSNPs can further target the disease tissues via the SR-A-mediated, active targeting to RA.

3.4. *In vivo* therapeutic efficacy of MTX-DSNPs

To evaluate the anti-inflammatory effects of MTX-DSNPs, the clinical scores of the inflamed joints were determined in the CIA mice for 5 weeks after the first immunization. The forelimb and hindlimb joints of the CIA mice were assigned clinical scores on a scale ranging from 0 to 4 to reflect the severity of inflammation and swelling. MTX-DSNPs (2.5 mg/kg of MTX) were administrated every 3 days into the tail vein of each mouse. Vehicle (PBS, pH 7.4), non-loaded DSNP, and free-MTX (2.5 mg/kg of MTX) were used as controls. The vehicle-treated group exhibited serious inflammation of the joints after 24 days, as reflected by the rapid increase in clinical score (Fig. 7a). Compared to the vehicle-treated group and non-loaded DSNPs-treated group, the free MTX-treated group showed much lower clinical scores for the entire duration of the experiment. Of particular note, the MTX-DSNP-treated group had the lowest clinical scores. Consistent with the inflammation results, the paw thickness was highest in the vehicle group, followed by the free MTX group and finally by the MTX-DSNP group (Fig. 7b). These data clearly indicate that the MTX-DSNPs significantly improved clinical outcomes, including arthritis indices and paw thickness. These therapeutic effects might result from passive and/or active targeting of the DSNPs, followed by the release of MTX.

To further evaluate the therapeutic efficacy of the MTX-DSNPs, histological analysis was performed on the knee joints of the vehicle-, DSNP-, MTX-, and MTX-DSNP-treated mice (Fig. 7c). The knee joints from vehicle-treated CIA mice showed inflammatory cell

infiltration, extensive synovitis and pannus formation, destruction of articular cartilage, and bone erosion. On the other hand, the knee joints from free MTX-treated CIA mice exhibited slightly less signs of inflammation. However, compared to the knee joints from free MTX-treated mice, the knee joints from MTX-DSNP-treated mice exhibited significantly reduced cartilage erosion, neutrophil infiltration, and synovial inflammation (Figs. 7d-f). In addition, histological analyses of major organs also demonstrated that there are no significant changes in major organs after administration of MTX-DSNP (Supplementary Fig. S6). These results are consistent with the therapeutic effects of the MTX-DSNPs.

3.5. Potential of DSNPs as an imaging probe for therapeutic monitoring

To further examine the therapeutic effects of the MTX-DSNPs, FPR-675-labeled DSNPs were intravenously injected into WT and CIA mice. Fluorescence signals from the nanoparticles were monitored at the knee joints after removal of the skin (Fig 8a). WT mice did not exhibit any FPR-675-DSNP fluorescence, indicating that DSNPs are not accessible to the normal tissue because the endothelial layer in the blood vessel acts as a diffusion barrier. However, strong FPR-675-DSNP fluorescence was observed in the inflamed legs of the non-treated CIA mice, presumably due to the accumulation of DSNPs in the inflamed joints via the leaky vasculature. Of particular note, weak fluorescence was observed in the legs of MTX-DSNP-treated CIA mice, implying minimal accumulation of DSNPs is needed to achieve therapeutic effects. Histological staining of CD31 was also performed to observe the blood vessel distribution *ex vivo* in the knee joint (Fig. 8b). Compared to WT and MTX-DSNP-treated CIA mice, non-treated CIA mice exhibited more CD31 (brown) expression. This finding implies that RA progression is involved in angiogenesis, which allows for

selective accumulation of DSNPs at the inflamed joint. Overall, our findings indicate that DSNPs can effectively deliver drugs to inflamed joints and are also potentially useful as optical probes for monitoring therapeutic efficacy in CIA mice.

4. Discussion

Nanomedicine has been exploited as potent therapeutics to improve pharmacokinetics and tissue-distribution of therapeutic agents over the past decades. In particular, it has been extensively studied for targeted cancer therapy because nano-sized structures passively accumulate into tumor tissues through leaky tumor vasculatures after systemic administration. Of note, since RA is also kwon as an angiogenesis-dependent disease, the passive targeting strategy has been applied to improve delivery efficiency of drugs to inflamed tissue for effective treatment of RA. Many types of nano-sized drug delivery systems such as liposomes, micellar and polymeric self-assemblies were employed to deliver anti-inflammatory drugs to the inflamed regions by the passive targeting strategy [32, 33]. However, only a few studies demonstrated active targeting approaches to treatment of RA *in vivo* [34-36]. In the previous studies, nanoparticles modified with targeting moieties such as a vasoactive intestinal peptide, folate and anti-CD64 antibody were used for the targeted deliver of anti-inflammatory drugs to inflamed tissues of RA *in vivo*. To date, however, DS-based nanomedicine has not been demonstrated for targeted drug delivery to RA *in vivo*.

Herein, we report a RA-targeted drug delivery system based on an amphiphilic DS conjugate, where DS is employed as a hydrophilic polymer backbone as well as a receptor-mediated, active targeting ligand to improve targetability of the system to RA tissues. Since SR-A receptor proteins are upregulated by the inflamed cells in RA synovial tissues such as

activated macrophage and lymphocytes, it is expected that DSNPs can actively permeate into the inflamed cells, preceded by a passive accumulation of DSNPs in the RA tissues. As evident from the imaging studies, DSNPs precisely target inflamed tissues of experimental CIA model (12-fold at ankles, 6-fold at knees), and were selectively internalized into inflamed cells; however, they did not show significant accumulation in the normal tissues of WT mice and cellular uptake into the control cells without inflammation (Fig. 4,5).

Importantly, we further scrutinized the targeting mechanism of DNSPs to RA tissues by following methods. (i) First, we monitored the cellular uptake of DSNPs at different temperature (4^oC and 37^oC) to understand if the internalization of DSNPs relies on the energy-dependent mechanism. Internalization of DSNPs into the inflamed cells was significantly impeded at low temperature (4^oC) compared to that at 37^oC (Fig. 3a and Supplementary Fig. S5). (ii) Second, we studied the internalization mechanism of DSNPs via the competitive inhibition study. Cellular uptake of DSNPs was monitored in the inflamed cells upregulated with SR-A receptors as well as in the cells on which SR-A receptors were preoccupied with DS polymers as a competitive inhibitor. Internalization of DSNPs into the inflamed cells were selectively inhibited with the SR-A receptor blocked by the pretreatment of the DS polymer (Fig. 3b). The results clearly indicate that cellular uptake of DSNPs into the inflamed cells is based on the energy-dependent and SR-A mediated mechanism. (ii) Moreover, we investigated the targeting mechanism of DSNPs by comparing *in vitro* cellular uptake and *in vivo* RA-targeting of DSNPs with those of non-targeted Dex-NPs. Interestingly, DSNPs showed significantly higher accumulation at the inflamed joints (2-fold) than non-targeted Dex-NPs (Fig. 6). These results imply that both DSNPs and Dex-NPs can accumulate at inflamed joints by the passive targeting mechanism, but DSNPs can further

accumulate and stay longer at the disease tissue owing to the SR-A- mediated, active targeting mechanism of DSNPs than Dex-NPs can. Thanks to excellent targeting of DSNPs to RA, they could facilitate delivery of MTX to the disease tissues and subsequently lead to excellent therapeutic outcomes (Fig. 7,8).

5. Conclusion

An amphiphilic DS derivative, capable of forming stable nano-sized particles and specifically binding to SR-A on the activated macrophages, was prepared to investigate its potential as a targeted nanomedicine for RA. The prepared DSNPs were readily taken up by activated macrophages via SR-A-mediated endocytosis. Systemically administrated DSNPs accumulated selectively in the inflamed tissue of RA, which was due to passive and active targeting mechanisms. MTX-loaded DSNPs had significantly improved therapeutic efficacy *in vivo* compared to free MTX. Overall, DSNPs have potential as MTX carriers and as imaging probes for RA.

Acknowledgments

This work was financially supported by the Korea Healthcare Technology R&D Project (HI14C03810200) of MW and the Basic Science Research Program (2015R1A2A2A05001390) of NRF.

References

[1] Lee DM, Weinblatt ME. Rheumatoid arthritis. The Lancet. 358 (2001) 903-911.
[2] Maruotti N, Cantatore F, Crivellato E, Vacca A, Ribatti D. Macrophages in rheumatoid arthritis. Histol. Histopathol. 22 (2007) 581-586.
[3] Smolen JS, Steiner G. Therapeutic strategies for rheumatoid arthritis. Nat. Rev. Drug Discovery. 2 (2003) 473-488.
[4] Davignon J-L, Hayder M, Baron M, Boyer J-F, Constantin A, Apparailly F, et al. Targeting monocytes/macrophages in the treatment of rheumatoid arthritis. Rheumatology. 52 (2013) 590-598.
[5] Kinne RW, Bräuer R, Stuhlmüller B, Palombo-Kinne E, Burmester G-R. Macrophages in rheumatoid arthritis. Arthritis Res. Ther. 2 (2000) 189-202.
[6] McInnes IB, Schett G. Cytokines in the pathogenesis of rheumatoid arthritis. Nat. Rev. Immunol. 7 (2007) 429-442.
[7] Cronstein BN. Low-dose methotrexate: a mainstay in the treatment of rheumatoid arthritis. Pharmacol. Rev. 57 (2005) 163-172.
[8] Mount C, Featherstone J. Rheumatoid arthritis market. Nat. Rev. Drug Discovery. 4 (2005) 11-12.
[9] Lee GY, Kim J-H, Choi KY, Yoon HY, Kim K, Kwon IC, et al. Hyaluronic acid nanoparticles for active targeting atherosclerosis. Biomaterials. 53 (2015) 341-348.
[10] Thambi T, Deepagan V, Yoon HY, Han HS, Kim S-H, Son S, et al. Hypoxia-responsive polymeric nanoparticles for tumor-targeted drug delivery. Biomaterials. 35 (2014) 1735-1743.
[11] Yoon HY, Koo H, Choi KY, Kwon IC, Choi K, Park JH, et al. Photo-crosslinked hyaluronic acid nanoparticles with improved stability for in vivo tumor-targeted drug delivery. Biomaterials. 34 (2013) 5273-5280.
[12] Ju E, Liu Z, Du Y, Tao Y, Ren J, Qu X. Heterogeneous assembled nanocomplexes for ratiometric detection of highly reactive oxygen species in vitro and in vivo. ACS nano. 8 (2014) 6014-6023.
[13] Levick JR. Permeability of rheumatoid and normal human synovium to specific plasma proteins. Arthritis Rheum. 24 (1981) 1550-1560.
[14] Kim MJ, Park J-S, Lee SJ, Jang J, Park JS, Back SH, et al. Notch1 targeting siRNA delivery nanoparticles for rheumatoid arthritis therapy. J. Controlled Release. 216 (2015) 140-148.
[15] Chen Z, Liu Z, Li Z, Ju E, Gao N, Zhou L, et al. Upconversion nanoprobes for efficiently in vitro imaging reactive oxygen species and in vivo diagnosing rheumatoid arthritis. Biomaterials. 39 (2015) 15-22.
[16] Kobayashi T, Ishida T, Okada Y, Ise S, Harashima H, Kiwada H. Effect of transferrin receptor-targeted liposomal doxorubicin in P-glycoprotein-mediated drug resistant tumor cells. Int. J. Pharm. 329 (2007) 94-102.
[17] Choi KY, Chung H, Min KH, Yoon HY, Kim K, Park JH, et al. Self-assembled hyaluronic acid nanoparticles for active tumor targeting. Biomaterials. 31 (2010) 106-114.
[18] Kodama T, Freeman M, Rohrer L, Zabrecky J, Matsudaira P, Krieger M. Type I macrophage scavenger receptor contains α-helical and collagen-like coiled coils. Nature. 343 (1990) 531-535.
[19] Li AC, Glass CK. The macrophage foam cell as a target for therapeutic intervention. Nat. Med. 8 (2002) 1235-1242.

[20] Kodama T, Reddy P, Kishimoto C, Krieger M. Purification and characterization of a bovine acetyl low density lipoprotein receptor. Proc.Natl. Acad. Sci. 85 (1988) 9238-9242.
[21] Kim S-H, Kim J-H, You DG, Saravanakumar G, Yoon HY, Choi KY, et al. Self-assembled dextran sulphate nanoparticles for targeting rheumatoid arthritis. Chem. Comm. 49 (2013) 10349-10351.
[22] Thambi T, You DG, Han HS, Deepagan V, Jeon SM, Suh YD, et al. Bioreducible Carboxymethyl Dextran Nanoparticles for Tumor-Targeted Drug Delivery. Adv. Healthcare Mater. 3 (2014) 1829-1838.
[23] You DG, Deepagan V, Um W, Jeon S, Son S, Chang H, et al. ROS-generating TiO2 nanoparticles for non-invasive sonodynamic therapy of cancer. Sci. Rep. 6 (2016) 23200.
[24] You DG, Saravanakumar G, Son S, Han HS, Heo R, Kim K, et al. Dextran sulfate-coated superparamagnetic iron oxide nanoparticles as a contrast agent for atherosclerosis imaging. Carbohydr. Polym. 101 (2014) 1225-1233.
[25] Platt N, Suzuki H, Kurihara Y, Kodama T, Gordon S. Role for the class A macrophage scavenger receptor in the phagocytosis of apoptotic thymocytes in vitro. Proc. Natl. Acad. Sci. 93 (1996) 12456-12460.
[26] Tu C, Ma X, Pantazis P, Kauzlarich SM, Louie AY. Paramagnetic, silicon quantum dots for magnetic resonance and two-photon imaging of macrophages. J. Am. Chem. Soc. 132 (2010) 2016-2023.
[27] Courtenay J, Dallman MJ, Dayan A, Martin A, Mosedale B. Immunisation against heterologous type II collagen induces arthritis in mice. Nature. 283 (1980) 666-668.
[28] Ellis J, Chain B, Cooke A, Ibrahim M, Katz D. Adjuvant Composition Determines the Induction of Type II Collagen-Induced Arthritis. Scand. J. Immunol. 36 (1992) 49-56.
[29] Brand DD, Latham KA, Rosloniec EF. Collagen-induced arthritis. Nat. Protoc. 2 (2007) 1269-1275.
[30] Jeon S, Ko H, Rao NV, Yoon HY, You DG, Han HS, et al. A versatile gold cross-linked nanoparticle based on triblock copolymer as the carrier of doxorubicin. RSC Adv. 5 (2015) 70352-70360.
[31] Fitzgerald ML, Moore KJ, Freeman MW, Reed GL. Lipopolysaccharide induces scavenger receptor A expression in mouse macrophages: a divergent response relative to human THP-1 monocyte/macrophages. J. Immunol. 164 (2000) 2692-2700.
[32] van den Hoven JM, Van Tomme SR, Metselaar JM, Nuijen B, Beijnen JH, Storm G. Liposomal drug formulations in the treatment of rheumatoid arthritis. Mol. Pharmaceutics. 8 (2011) 1002-1015.
[33] Ulmansky R, Turjeman K, Baru M, Katzavian G, Harel M, Sigal A, et al. Glucocorticoids in nano-liposomes administered intravenously and subcutaneously to adjuvant arthritis rats are superior to the free drugs in suppressing arthritis and inflammatory cytokines. J. Controlled Release. 160 (2012) 299-305.
[34] Thomas TP, Goonewardena SN, Majoros IJ, Kotlyar A, Cao Z, Leroueil PR, et al. Folate-targeted nanoparticles show efficacy in the treatment of inflammatory arthritis. Arthritis Rheum. 63 (2011) 2671-2680.
[35] Sethi V, Rubinstein I, Kuzmis A, Kastrissios H, Artwohl J, Onyuksel H. Novel, biocompatible, and disease modifying VIP nanomedicine for rheumatoid arthritis. Mol. Pharmaceutics. 10 (2013) 728-738.
[36] Heo R, Park J-S, Jang HJ, Kim S-H, Shin JM, Suh YD, et al. Hyaluronan nanoparticles bearing γ-secretase inhibitor: in vivo therapeutic effects on rheumatoid arthritis. J. Controlled

Release. 192 (2014) 295-300.

Figure captions

Fig. 1. Schematic illustration of DSNPs as nanocarriers for targeted RA therapy.

Fig. 2. (a) Synthesis of the amphiphilic DS derivative. (b) Size distributions of the DSNPs and MTX-DSNPs in distilled water at 25^{o}C. Insert TEM images of the nanoparticles. Scale bar, 700 nm. (c) *In vitro* release profile of MTX from DSNPs in PBS (pH 7.4). Error bars represent the standard deviation (n = 5).

Fig. 3. *In vitro* cellular uptake of DSNPs. (a) Confocal microscope images of RAW264.7 (LPS, -) macrophages, RAW264.7 (LPS, +) macrophages, and BAECs incubated with FPR-675-labeled DSNPs are shown. (b) SR-A-mediated endocytosis of DSNPs. The confocal microscope images of RAW264.7 (LPS, +/ free DS, -/DSNPs), RAW264.7 (LPS, +/ free DS, +/DSNPs), and RAW264.7 (LPS, +/ free DS, -/Dex-NPs). Scale bar, 50 μm.

Fig. 4. Biodistribution of FPR-675-labeled DSNPs in mice. (a) Time-dependent NIRF images of whole hind legs of WT and CIA mice. (b) *Ex vivo* NIRF images of various organs in WT and CIA mice. (c) Quantification of DSNP fluorescence intensity in each organ. Error bars represent the standard deviation (n = 3). $^{***}P < 0.001$.

Fig. 5. Activated macrophage-targeting ability of DSNPs. (a) Distribution of DSNPs and SR-A in the synovia of WT and CIA mice. SR-A expression was examined using immunohistochemistry. Scale bar, 50 μm. (b) Quantification of DSNP and SR-A fluorescence intensities in the synovium. Error bars represent the standard deviation (n = 3).

Fig. 6. Biodistribution of FPR-675-labeled DSNP and FPR-675-labeled Dex-NP in mice. (a) Time-dependent images of whole hind legs of CIA mice. (b) Quantification of fluorescence intensity after intravenous administration of both nanoparticles. Error bars represent the standard deviation (n = 3). $^{***}P < 0.001$.

Fig. 7. Therapeutic efficacy of MTX-DSNPs. (a) The severity of arthritis was determined using a visual arthritis scoring system for CIA mice treated with vehicle, DSNP, MTX, or MTX-DSNPs. Error bars represent the standard error (n = 10). (b) Paw thicknesses were measured using calipers. Error bars represent the standard deviation (n = 10). (c) H&E staining of knee joints excised from the mice. Scale bar, 200 μm. Histological scores of (d) cartilage erosion, (e) neutrophil infiltration, and (f) synovial inflammation are shown. Error bars represent the standard error (n = 5). $^{***}P < 0.001$, $^{*}P < 0.05$ compared with vehicle. $^{###}P < 0.001$, $^{##}P < 0.01$ compared with Free-MTX. This figure is representative images of repeated experiments (n = 3).

Fig. 8. NIRF imaging of the therapeutic effect of MTX-DSNPs in CIA mice. (a) *In vivo* NIRF images of joints of the WT and CIA mice. NIRF images were obtained at 12 h post-injection of FPR-675-labeled DSNPs. Scale bar, 500 μm. (b) Distribution of CD31 in WT and CIA mice. CD31 (brown) expression was analyzed by immunohistochemistry. Scale bar, 100 μm.

Table 1. Physicochemical characteristics of the DSNPs.

Sample	Size (nm)[a]	Zeta potential (mv)[a]	Encapsulation efficiency (%)[b]	Drug loading (μg/mg)[b]
DSNP	220.0 ± 5.17	-47.52 ± 1.26	-	-
DSNP-MTX	173.4 ± 4.12	-43.64 ± 2.37	73.05	73.05

[a] Measured by using a Zeta-sizer (n = 5).
[b] Measured by using a UV–vis spectrophotometer.

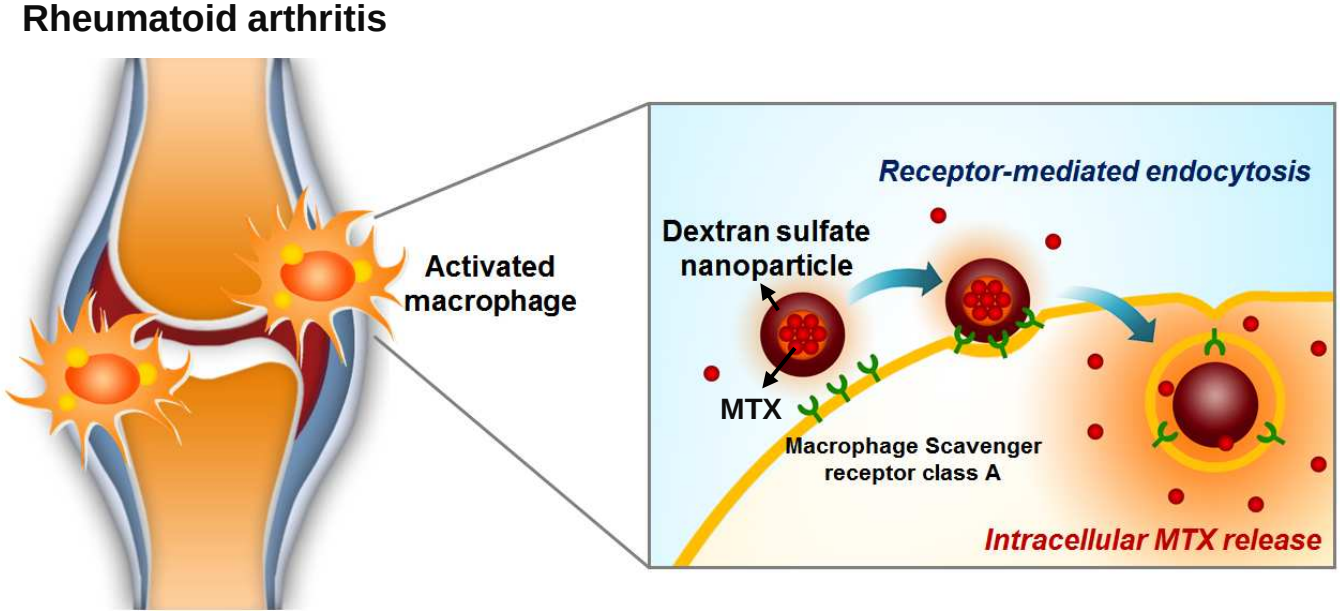

Figure 1. Heo et al.

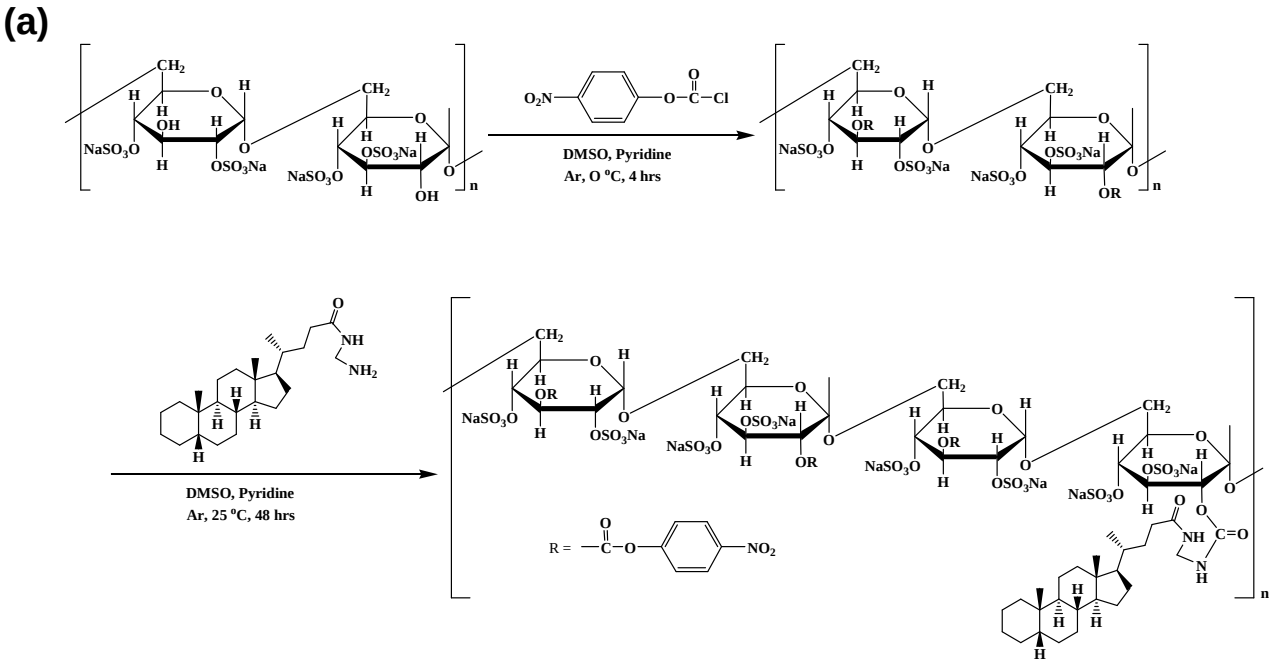

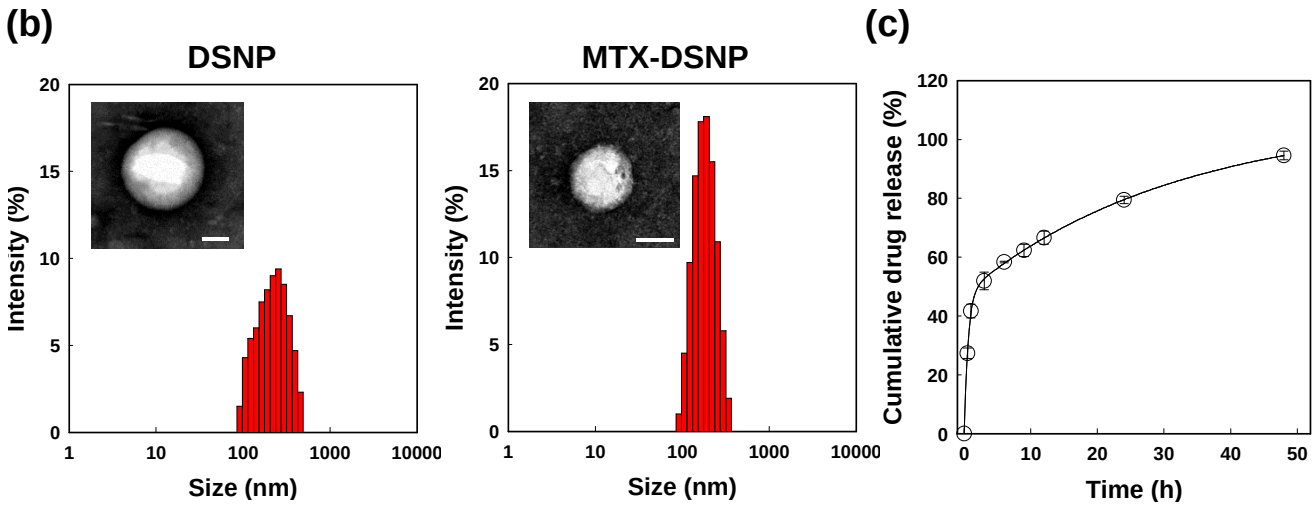

Figure 2. Heo et al.

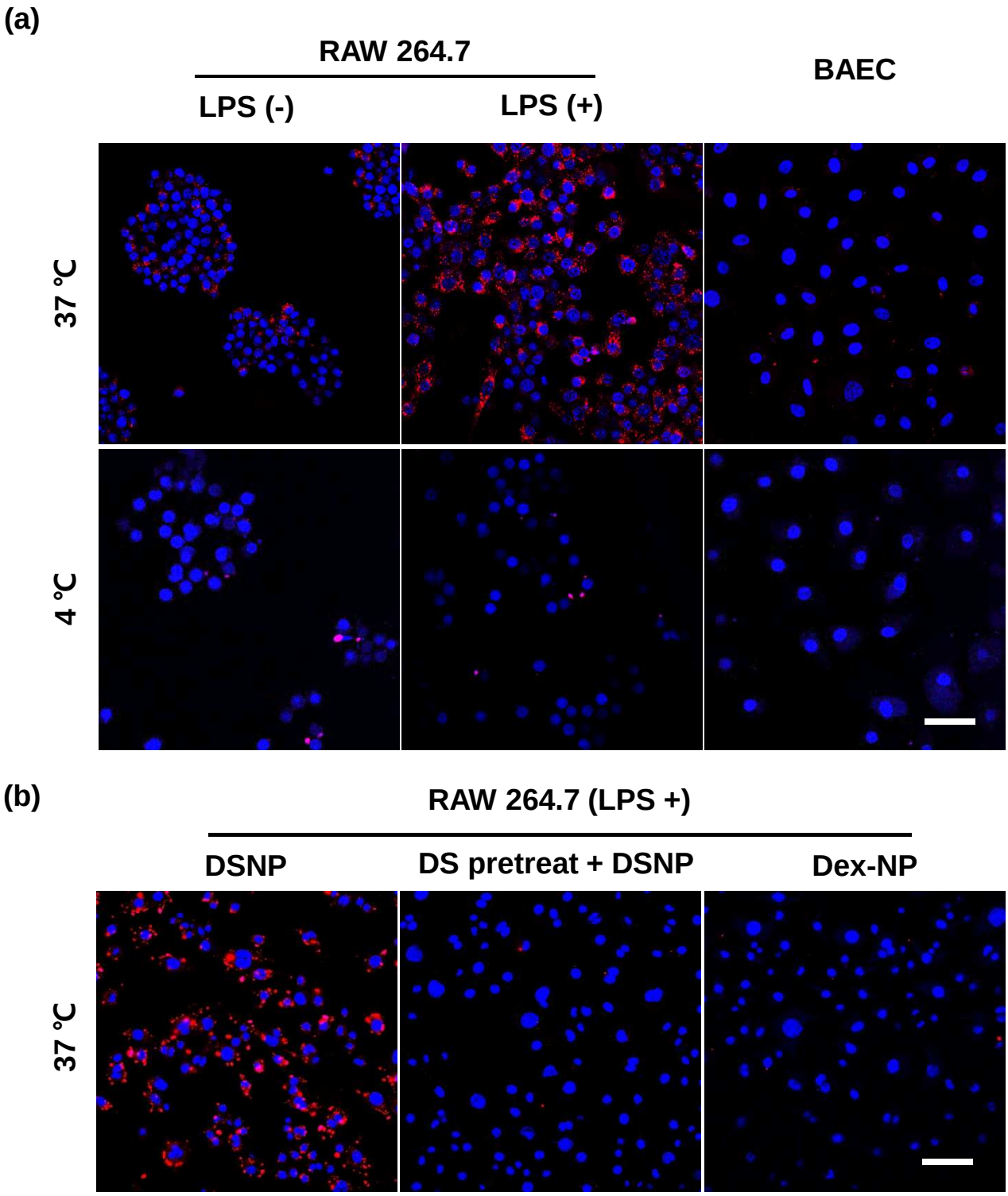

Figure 3. Heo et al.

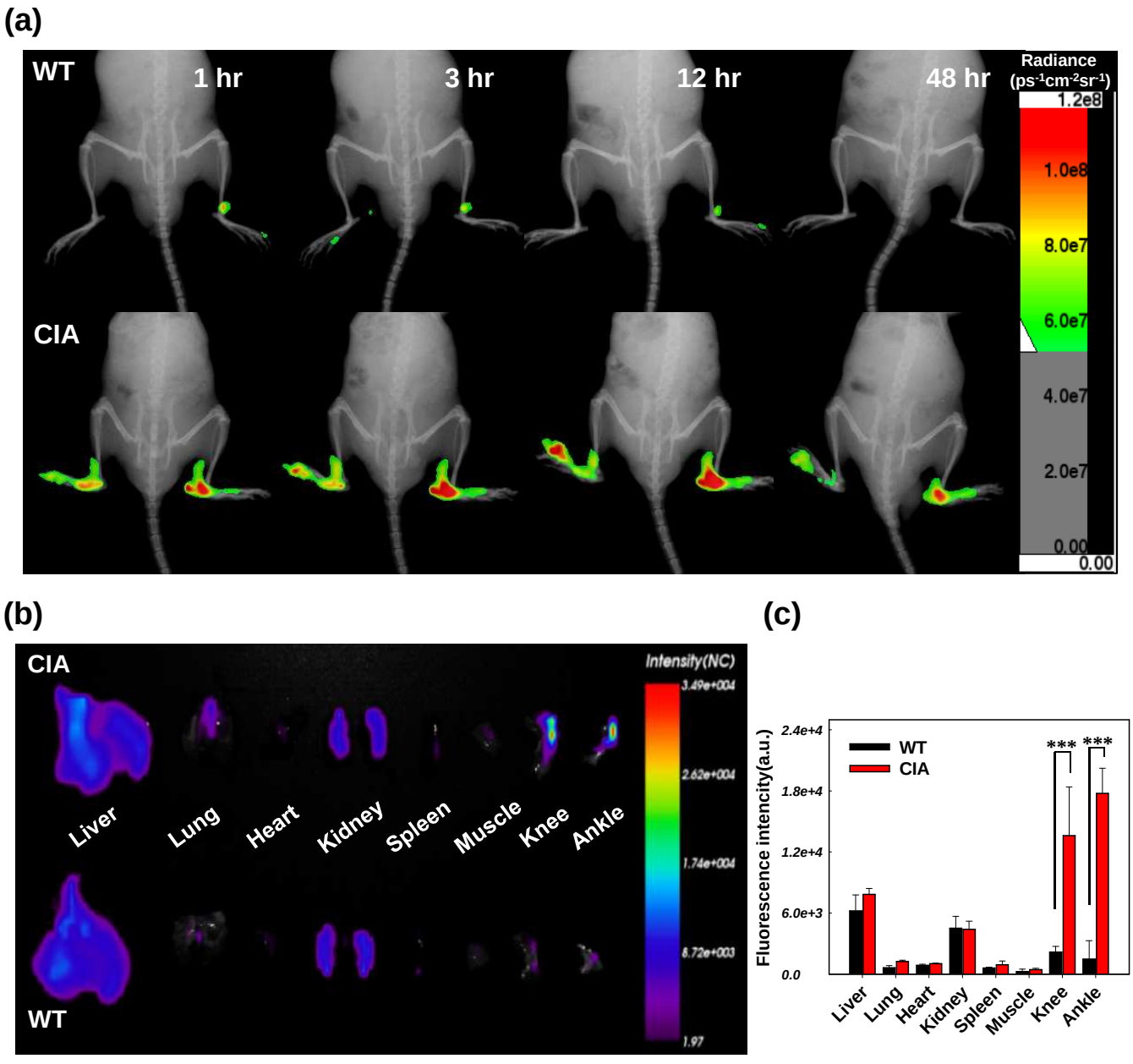

Figure 4. Heo et al.

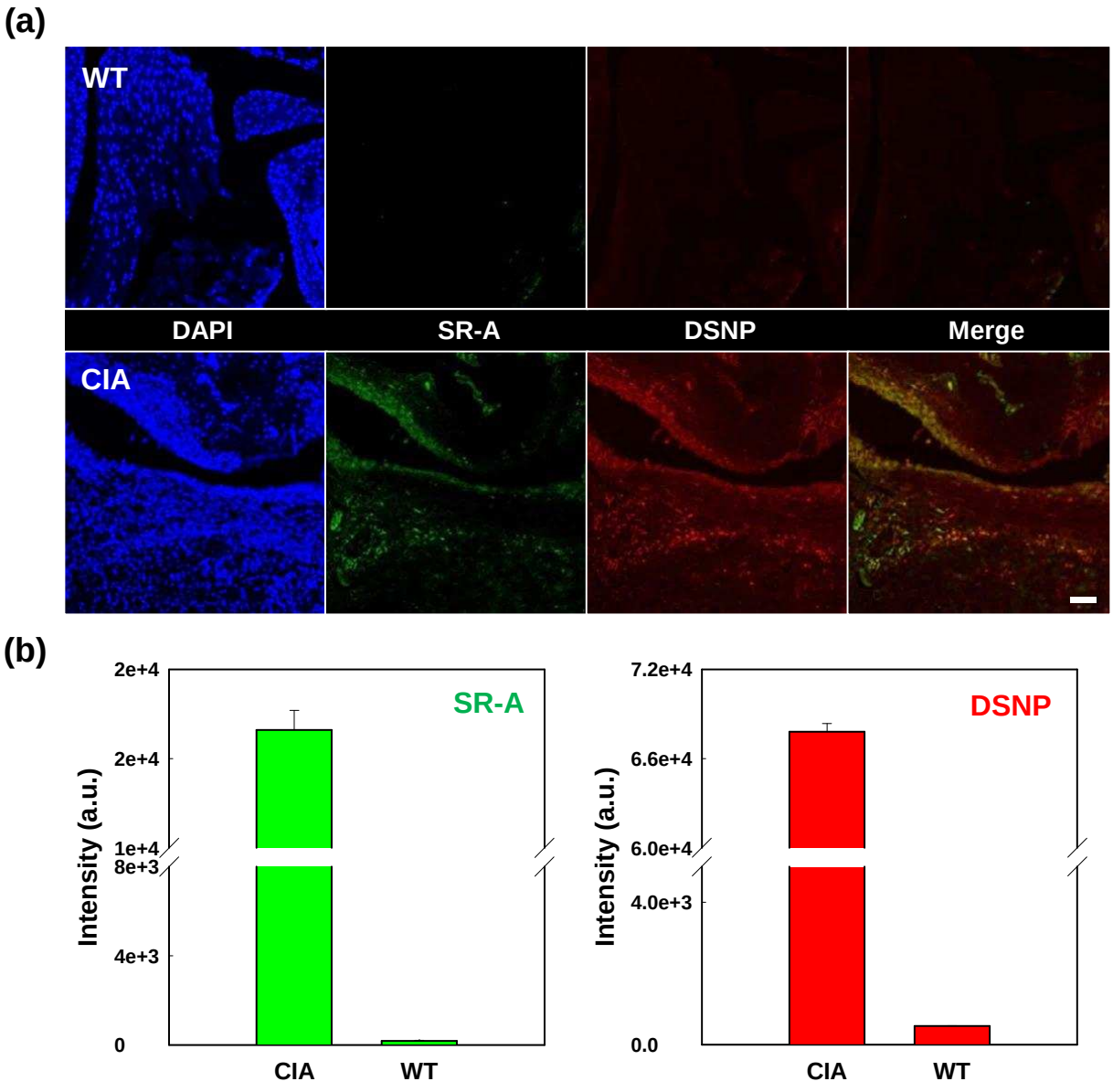

Figure 5. Heo et al.

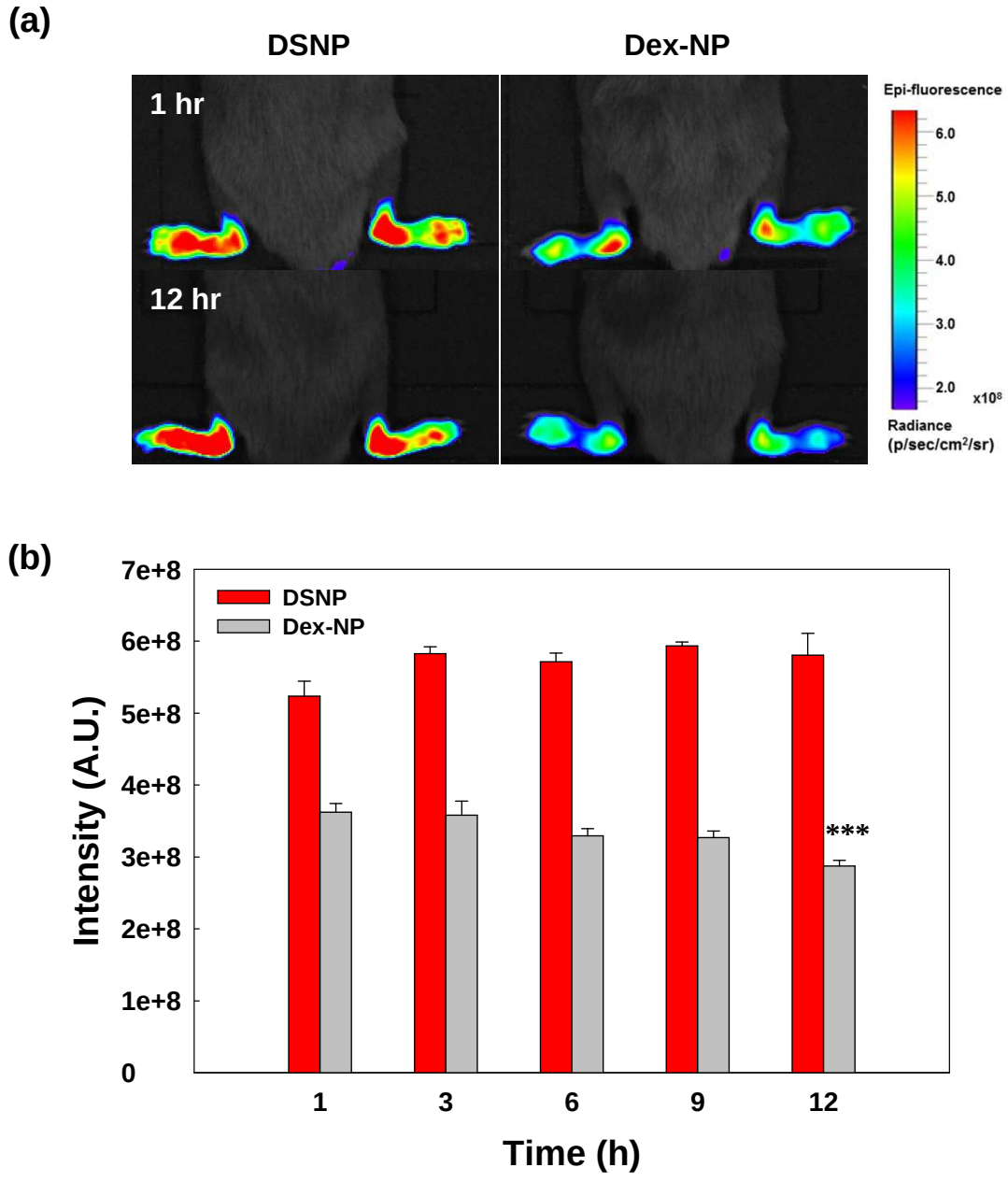

* : $p < 0.001$

Figure 6. Heo et al.

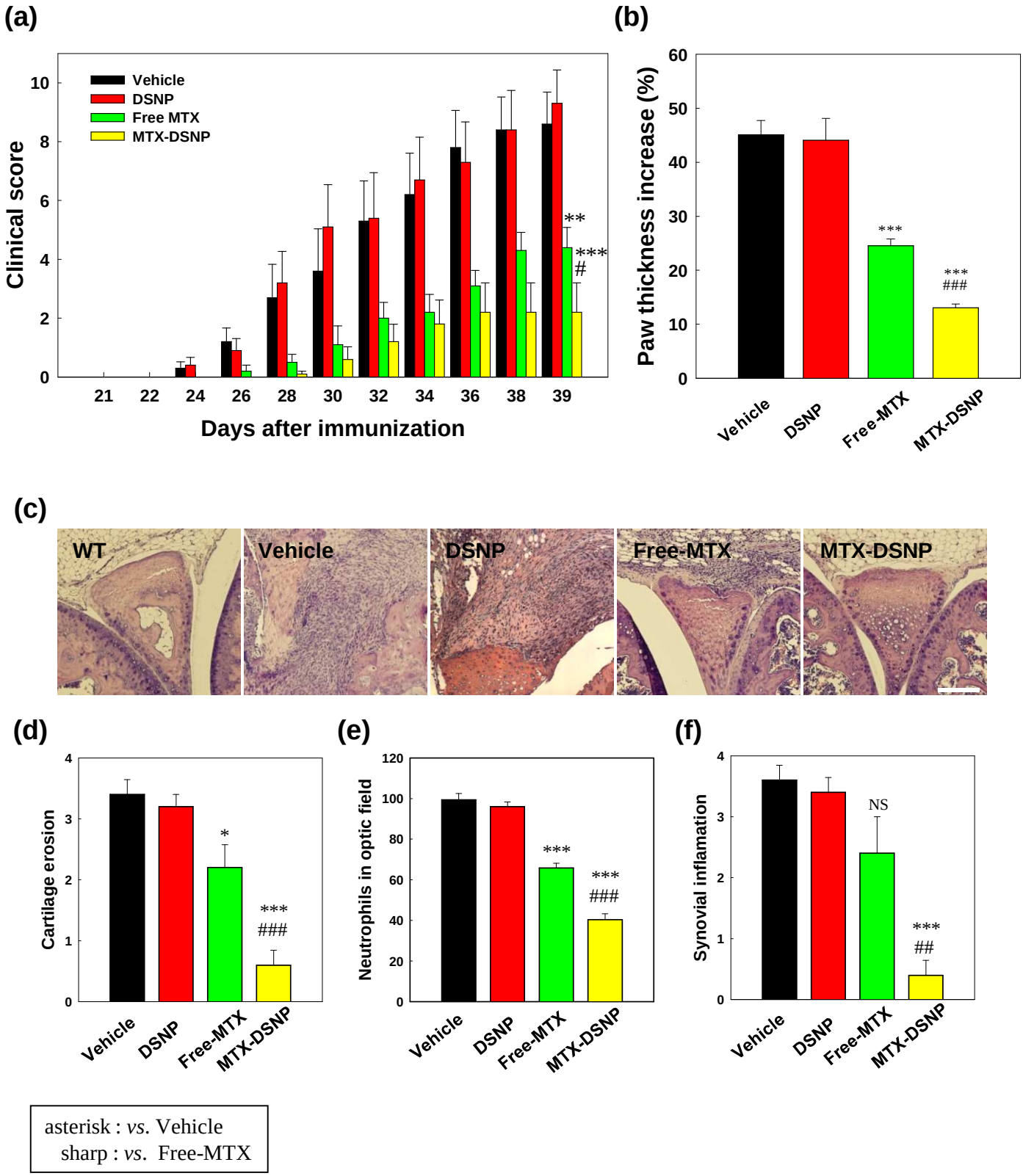

Figure 7. Heo et al.

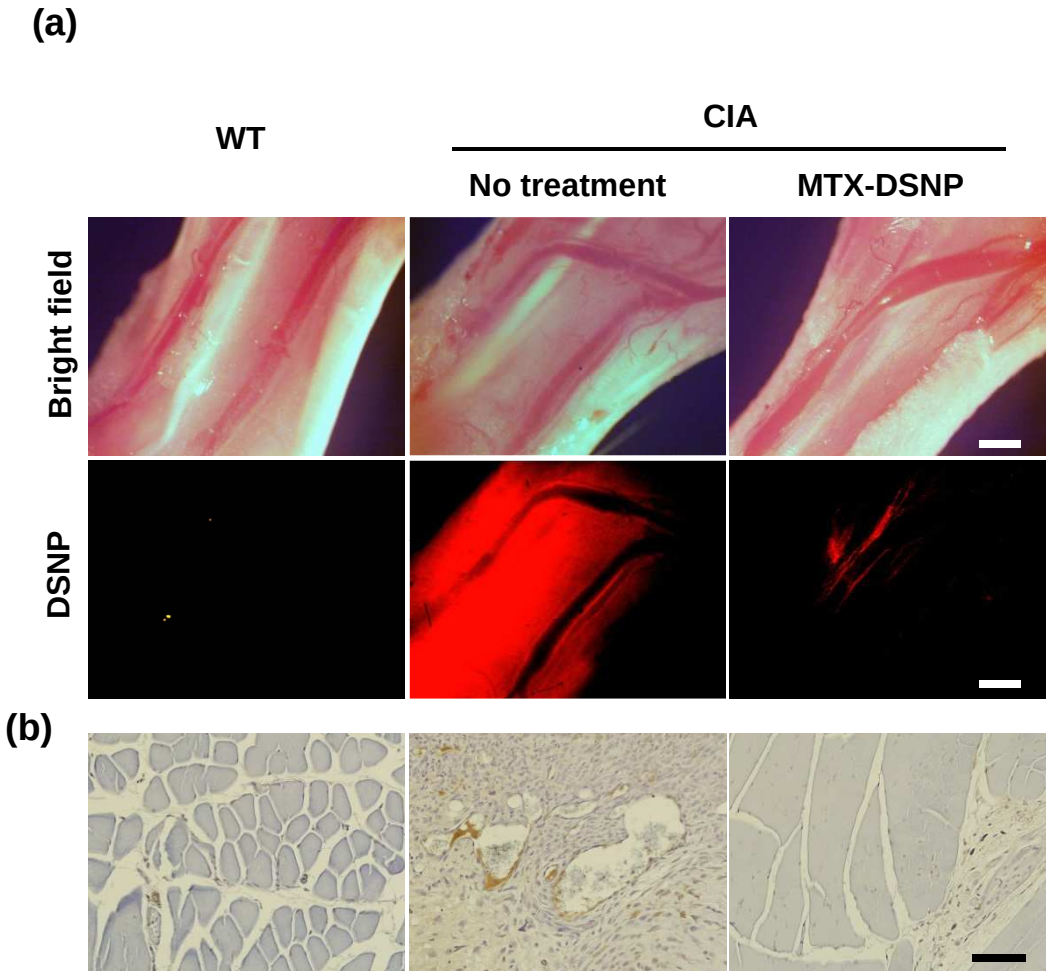

Figure 8. Heo et al.